THE GEOLOGICAL SOCIETY OF AMERICA®

Radioisotopic age, osmium isotopes, and global correlation of the Albian-Cenomanian boundary

Brad S. Singer[1,2,†], Reishi Takashima[2], Youjuan Li[1,*], Mark D. Schmitz[3], David Selby[4], Bradley B. Sageman[5], Luca G. Podrecca[5], Hiroshi Nishi[6], Brian R. Jicha[1], and Toshiro Yamanaka[7]

[1]*Department of Geoscience, University of Wisconsin–Madison, Madison, Wisconsin 53706, USA*
[2]*Tohoku University Museum, Tohoku University, Aoba-ku, Sendai 980-8578, Japan*
[3]*Department of Geosciences, Boise State University, Boise, Idaho 83725, USA*
[4]*Department of Earth Science, Durham University, Durham DH1 3LE, UK*
[5]*Department of Earth and Planetary Sciences, Northwestern University, Evanston, Illinois 60208, USA*
[6]*Institute of Dinosaur Research, Fukui Prefectural University, 4-1-1, Matsuokakenjojima, Eiheiji-cho, Yoshida-gun, Fukui 910-1142, Japan*
[7]*School of Marine Resources and Environment, Tokyo University of Marine Science and Technology, 4-5-7, Konan, Minato-ku, Tokyo 108-847, Japan*

ABSTRACT

Zircon U-Pb and sanidine $^{40}Ar/^{39}Ar$ dates of individual crystals from 11 tuffs in sections of the Yezo Group, Hokkaido, Japan, yield an age for the Albian-Cenomanian boundary of 100.74 ± 0.10 Ma. This age, which exceeds that in the current geologic time scale (GTS2020) by 240 k.y., relies on correlation of distinctive positive $\delta^{13}C$ excursions known as the Albian-Cenomanian boundary event from the global stratotype section and point (GSSP) near Mont Risou, France, to those identified within Yezo Group strata. We find that the Albian-Cenomanian boundary in the Yezo Group is associated with a sharp negative $\delta^{13}C$ excursion as well as the onset of a progressive transition toward less radiogenic Os isotope ($^{187}Os/^{188}Os$) ratios. The subdued expression of the Albian-Cenomanian boundary event $\delta^{13}C$ isotope excursions, and that of oceanic anoxic event (OAE) 1d, relative to those of OAE1a and OAE2, coupled with a lack of prior evidence for an Os isotope shift, has led to the inference that monsoons, rather than submarine volcanism, propelled the lesser mid-Cretaceous OAEs. The high-resolution Os isotope profile of the Albian-Cenomanian boundary event from the Yezo Group provides potential evidence that submarine volcanism, likely associated with a high-flux phase of Kerguelen Plateau growth, played a role in perturbing the ocean carbon reservoir beginning during the final ~100,000 yr of the Albian stage. If the modest Os isotope shift reflects a volcanic source, its impact on seawater Os isotope composition was modulated by a drop in atmospheric and sea-surface temperatures, and a decrease in continental weathering at a global sequence boundary, features that distinguish the Albian-Cenomanian boundary event and OAE1d from the more prominent OAE1a and OAE2.

INTRODUCTION

Precise and accurate radioisotopic dating of sedimentary successions, including stage boundaries where possible, is important in testing and anchoring astronomical age models that are increasingly being used to gauge the timing and pace of environmental and biological events during the Cretaceous Period (e.g., Malinverno et al., 2010; Meyers et al., 2012; Sageman et al., 2014; Gambacorta et al., 2019; Ma et al., 2019; Leandro et al., 2022). The Albian-Cenomanian stage boundary is notable because it demarcates a paleoceanographic transition from deposition of marl-predominant sediment to mainly limestone that distinguishes the Early Cretaceous from the Late Cretaceous (e.g., Gale et al., 1996). The global stratotype section and point (GSSP) for the base of the Cenomanian is near Mont Risou, France, where, owing to sparsity of ammonites, the first appearance of the foraminifera *Thalmanninella globotruncanoides* (Sigal, 1948) is taken to define the Albian-Cenomanian stage boundary (Gale et al., 2020). Another distinguishing feature is a succession of four positive $\delta^{13}C$ excursions, each of about +0.2‰ to +0.5‰, that occur in uppermost Albian through lowermost Cenomanian strata (Gale et al., 1996; Jarvis et al., 2006). This succession comprises three excursions with peaks A, B, and C in uppermost Albian strata, followed by peak D in lowermost Cenomanian strata. This set of excursions has been called the Albian-Cenomanian boundary event (Gale et al., 2011). Notably, black shales including the Niveau Breistroffer succession in Tethyan sections, which span from the base of peak A to the termination of peak B, comprise oceanic anoxic event (OAE) 1d, which is also expressed by a modest short-lived negative $\delta^{13}C$ isotope excursion of 0.5‰ (Gale et al., 1996; Wilson and Norris, 2001; Bornemann et al., 2005; Gambacorta et al., 2015; Petrizzo and Gilardoni, 2020).

It has long been recognized that in the European Tethys, volcanic ash beds, which could provide a radioisotopic age for the Albian-Cenomanian boundary, are absent. Moreover, in the Western Interior Basin of North America, where dateable volcanic ash beds are abundant (Obradovich, 1993), ammonite fossils used to define the base of the Cenomanian stage are endemic, hampering global correlations. Turning instead toward strata of the Cretaceous Yezo Group in Hokkaido, Japan, Obradovich et al. (2002) determined $^{40}Ar/^{39}Ar$ ages from sanidine in two volcanic ash beds that occur within the ammonite zones of *Mantelliceras saxbii* and *Gray-*

Brad S. Singer https://orcid.org/0000-0003-3595-5168
†bsinger@wisc.edu
*Present address: Institute of Geology and Geophysics, Chinese Academy of Sciences, Beijing 100029, China

 https://doi.org/10.1130/B38503.1.

sonites wooldridgei. The age determined from the older of these two ash beds currently anchors the Albian-Cenomanian stage boundary age of 100.5 ± 0.5 Ma in the Geologic Timescale 2020 (GTS2020; Gale et al., 2020). Here, we explain how this age was derived from the data in Obradovich et al. (2002). Originally, these data were reported relative to an age for the neutron fluence standard mineral Fish Canyon sanidine of 28.02 Ma, yielding ages of the two ash beds of 98.98 ± 0.38 Ma and 99.16 ± 0.37 Ma (±2σ analytical uncertainty). These ages implied an age for the Albian-Cenomanian boundary of at least 99.2 ± 0.4 Ma, given that ~50 m of Cenomanian strata crop out below the older ash bed (Obradovich et al., 2002). If the Obradovich et al. (2002) ages are recalculated relative to a Fish Canyon sanidine age of 28.201 Ma (Kuiper et al., 2008), they become 99.64 ± 0.38 Ma and 99.82 ± 0.37 Ma. However, the latter age is based on six multicrystal aliquots of sanidine that exhibit considerable scatter among the individual dates, resulting in an unacceptably large mean square weighted deviation (MSWD) of 4.6. When the two youngest dates are excluded (first done implicitly by Cobban et al., 2006; J.D. Obradovich, 2008, personal commun.), the MSWD drops to 0.93, and the age becomes 100.01 ± 0.37 Ma (Singer et al., 2021).

Quidelleur et al. (2011) reported a U-Pb zircon age and $^{40}Ar/^{39}Ar$ biotite age of an ash bed (their sample SK069) from the lowermost Cenomanian Yezo Group strata that is stratigraphically proximal to the ash beds dated by Obradovich et al. (2002), but with uncertainty regarding correlation. The U-Pb zircon age of 99.7 ± 0.3 Ma in Quidelleur et al. (2011) derives from analysis of five multigrain aliquots using isotope dilution–thermal ionization mass spectrometry (ID-TIMS), whereas their $^{40}Ar/^{39}Ar$ biotite age of 100.2 ± 1.0 Ma is from a pair of disturbed age spectra that do not meet widely accepted plateau criteria (Schaen et al., 2021). Based on these results, Quidelleur et al. (2011) proposed that the base of the Cenomanian stage has a minimum age of 99.7 ± 0.3 Ma. As highlighted by Takashima et al. (2019) and Gale et al. (2020), because the ash beds dated by Obradovich et al. (2002) and Quidelleur et al. (2011) occur at the base of the *Mantelliceras saxbii* ammonite zone and above the first occurrence of the foraminifera *Thalmanninella globotruncanoides*, the current geologic time scale places the Albian-Cenomanian boundary at 100.5 ± 0.1 Ma, assuming that sediments underlying these ash beds were deposited during a single long eccentricity cycle of ~405 k.y. duration. Alternatively, on the basis of several $^{49}Ar/^{39}Ar$ sanidine ages determined from volcanic ash beds in the Western Interior Basin, including a tuff in the lowermost Cenomanian Shell Creek Shale in Montana that gives an age of 100.07 ± 0.07 Ma, in parallel with the Obradovich et al. (2002) age of 100.01 ± 0.37 Ma from Hokkaido, Singer et al. (2021, 2025) argued that the most appropriate age for the Albian-Cenomanian boundary is 100.00 ± 0.40 Ma.

Pronounced shifts toward unradiogenic $^{187}Os/^{188}Os$ ratios coincident with the negative $\delta^{13}C$ excursions associated with several mid-Cretaceous OAEs, including OAE1a, Wezel Level, Fallot Level, and OAE2, have led these events to be classified as volcanic-induced OAEs (Matsumoto et al., 2022). In contrast, the limited marine sediment data available that span OAE1c and OAE1d display no discernible $^{187}Os/^{188}Os$ shifts, prompting Matsumoto et al. (2022) to argue that these should be classified as monsoon-induced OAEs. However, a spike in the concentration of mercury, accompanied by a shift in its isotopic composition, occurs just below peak A of the Albian-Cenomanian boundary event in marine strata in the Youxia section, Tibet, with a modeled pCO_2 increase during peak B, which together are interpreted to imply that submarine volcanism played a role in driving OAE1d (Yao et al., 2021).

To further address uncertainties in the timing of the Albian-Cenomanian boundary associated with stratigraphic correlation to the GSSP in France and elsewhere, as well as the underlying driver of the Albian-Cenomanian boundary event, we present new lithostratigraphy and biostratigraphy, C and Os isotopic compositions, single-crystal $^{40}Ar/^{39}Ar$ sanidine dates, and single-crystal U-Pb zircon dates from Lower Cenomanian and Upper Albian strata of the Yezo Group in Hokkaido, Japan. We report new single-crystal $^{40}Ar/^{39}Ar$ and U-Pb ages from the tuffs dated by Obradovich et al. (2002) and Quidelleur et al. (2011), as well as from tuffs in three other sections. Our findings improve the accuracy of the boundary age, provide limits on the geologic and dating uncertainties, and improve correlations with strata of the Tethys and Western Interior Basin regions. The well-dated, high-resolution C and Os isotope record from Hokkaido also has implications for the cause of the Albian-Cenomanian boundary event and of OAE1d.

GEOLOGIC SETTING

The Yezo Group comprises ~10 km of terrigenous sandstone and mudstone intercalated with hundreds of silicic volcanic ash beds (tuffs) that were deposited in a marine forearc basin from the early Aptian to the Paleocene (Fig. 1; Takashima et al., 2019). In their review of the lithostratigraphy, biostratigraphy, and chronostratigraphy of the Yezo Group, Takashima et al. (2019) also presented new C isotope records from several key stratigraphic sections from which the tuffs we have dated were also collected (Fig. 2).

The Hikagenosawa Formation occurs in the middle part of the Yezo Group and correlates with the Upper Albian to Lower Cenomanian stages. The Hikagenosawa Formation is mainly composed of dark-gray mudstone with numerous silicic tuffs. However, a turbidite sandstone-predominant interval, named the Kanajiri Sandstone Member, is intercalated in the lower part of the Hikagenosawa Formation (Fig. 2). Sandstone beds in the Kanajiri Sandstone Member are thickest in the southern part of the Tomamae area (beds more than 1 m thick along the Kotanbetsu River), whereas the bed thickness decreases greatly, to 1–3 cm, toward the south and north. Based on macrofossils, planktic foraminifera, and C isotope stratigraphies, the Albian-Cenomanian boundary is placed in the Kanajiri Sandstone Member (Obradovich et al., 2002; Takashima et al., 2019).

MATERIALS AND METHODS

About 350 m of the Kyoei-Sakin-zawa section and 440 m of the Hotei-zawa section (Figs. 1A and 2), where the tuff beds R8943B and R8072 dated by Obradovich et al. (2002) crop out, were measured during two field campaigns with bulk mudstone samples collected every 3–10 m apart for C and Os isotope measurements (Fig. S1 in the Supplemental Material[1]). We also resampled tuff R8943B, as well as five other thin tuffs from the Kyoei-Sakin-zawa section for new $^{40}Ar/^{39}Ar$ and U-Pb dating analyses (Fig. 2). From a section along the Penkemoyuparo River in the Oyubari area (Fig. 1B), five tuff beds were sampled for dating analyses. Also for new dating, we resampled tuff HgSm-001 from the Shumarinai River section, which is equivalent to SK069 of Quidelleur et al. (2011), as well as tuffs HOT-002 (equivalent to tuff R8072 of Obradovich et al., 2002), HOT-003, and HOT-004 from the Hotei-zawa Creek section, and tuff Hiko-001 from a section along the Kotabetsu River (Figs. 1A and 2).

Biostratigraphy of the Kyoei-Sakin-zawa, Hotei-zawa, and Penkemoyuparo River Sections

Bulk mudstone samples from the Kyoei-Sakin-zawa (45 samples), Hotei-zawa (59

[1]Supplemental Material. Sampling profiles along rivers, photos of foraminifera, and complete C, Os, $^{40}Ar/^{39}Ar$, and U-Pb isotope data. Please visit https://doi.org/10.1130/GSAB.S.XXXX to access the supplemental material; contact editing@geosociety.org with any questions.

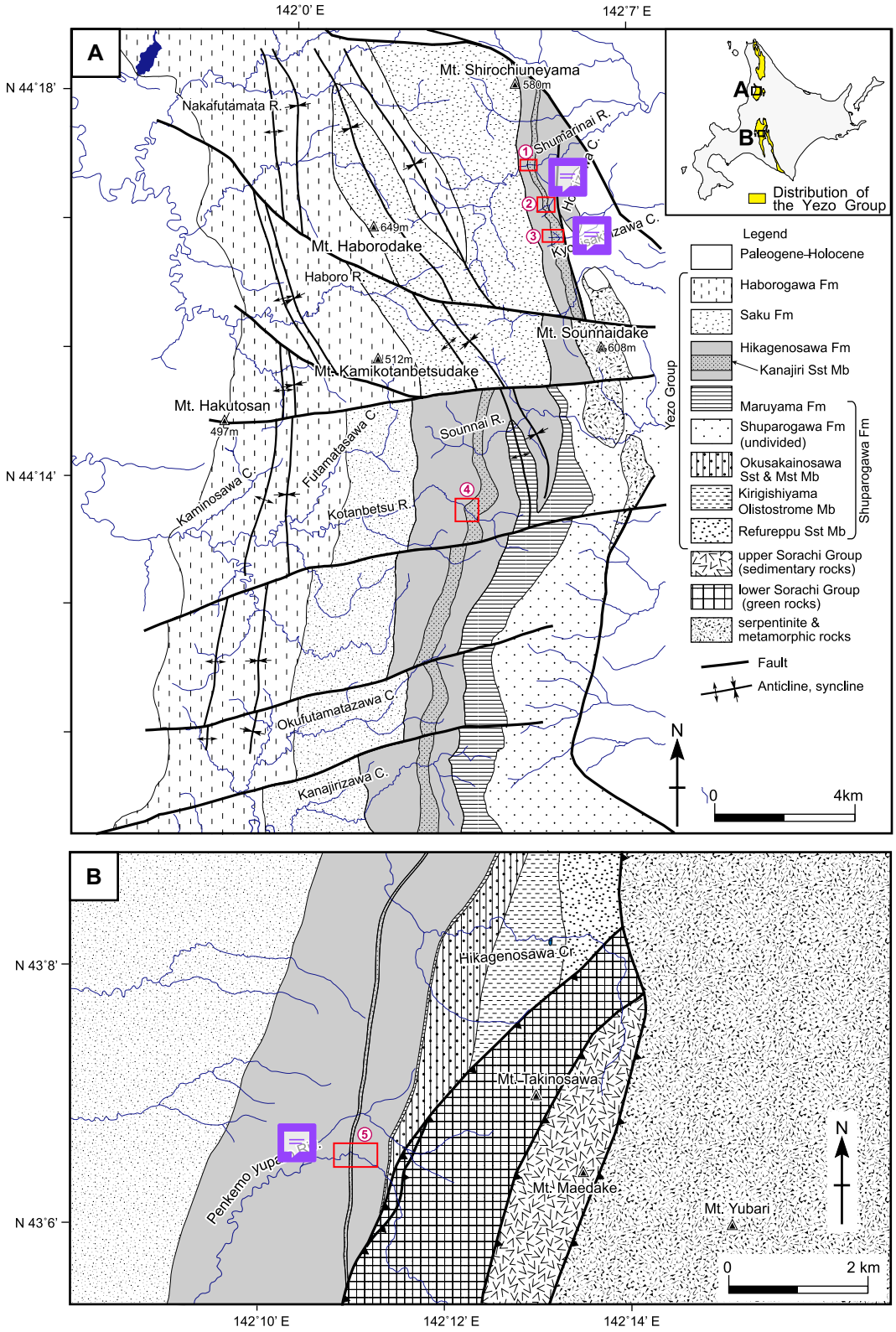

Figure 1. Geologic maps of the Yezo Group in the (A) Tomamae area and (B) Oyubari area, Japan, showing locations of five stratigraphic sections discussed in the main text. The sections comprise strata that are exposed along river channels and dip steeply to the west (Fig. S1, see text footnote 1). Sst—Sandstone; Mst—Mudstone; Mb—Member; R.—River; C—Creek.

samples), and Penkemoyuparo River (84 samples) sections were collected at 3 m to 15 m stratigraphic intervals for planktic foraminiferal biostratigraphy and C isotope stratigraphy analyses (Fig. S1). Dry sample aliquots of 400 g were disaggregated using sodium tetraphenylborate plus sodium chloride. The disaggregated sediment was washed over a 64 μm sieve and dried at 50 °C. All planktic foraminifera were removed from the washed residue, which comprised the >120 μm fraction. For megafossil biostratigraphy, we compiled data from Matsu-

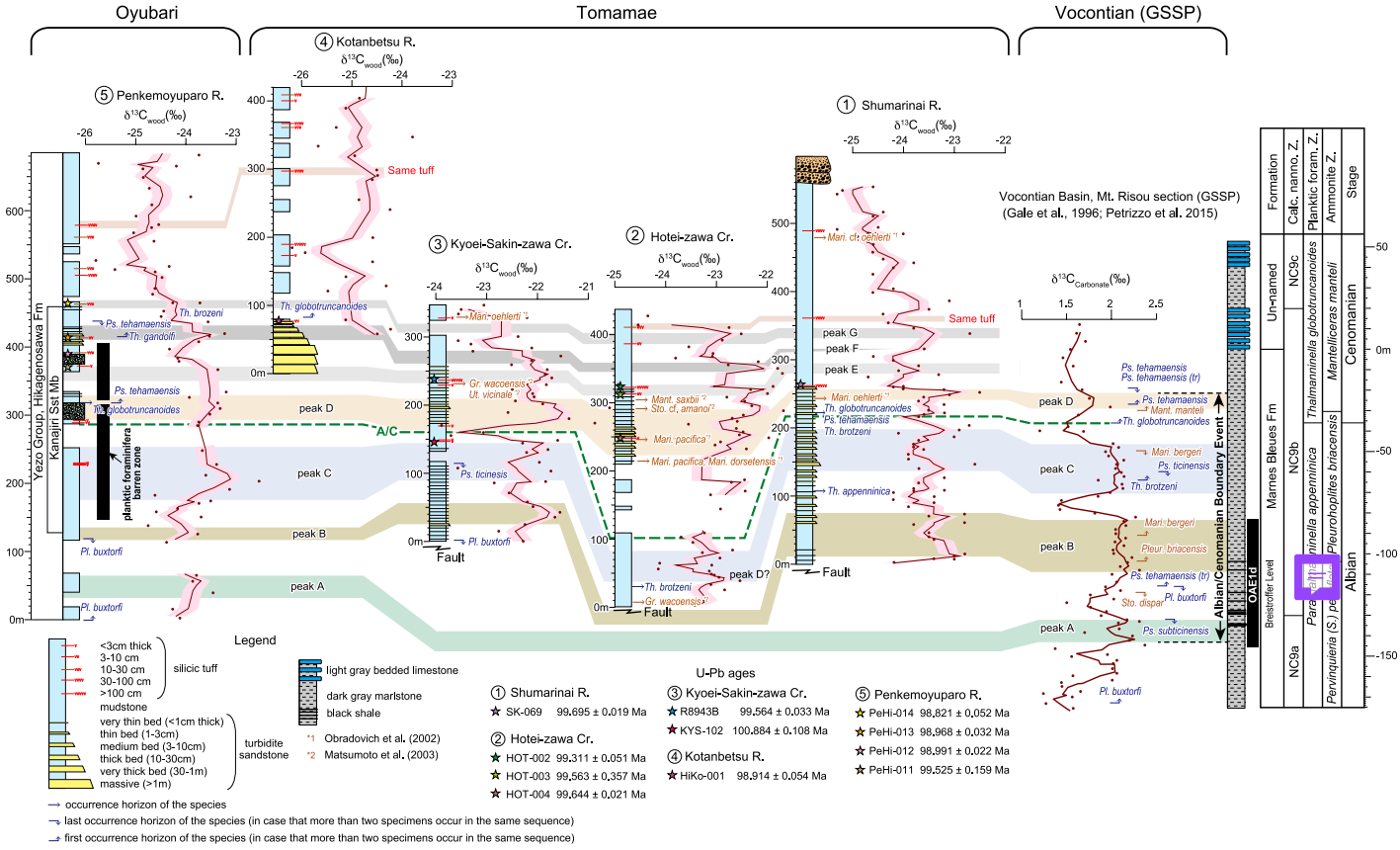

Figure 2. Correlation of five sections in the Yezo Group based on fossil occurrences and C isotope excursions discussed in the main text, with $^{206}Pb/^{238}U$ ages of 11 tuffs highlighted. Details of the Kyoei-Sakin-zawa section are illustrated in Figure 3. Brown profiles depict three-point moving averages of the $\delta^{13}C$ values in each section; pink envelopes encompass estimated ±1σ uncertainties. Albian-Cenomanian boundary is inferred to be at the green dashed line labeled A/C. Apatite compositions have been used to correlate tuff HgPk-019 between the Penkemoyuparu and Kotanbetsu River sections, and a different tuff HOT-008 between the Hotei-zawa and Shumarinai sections (Takashima et al., 2019). Ammonite zones for the Vocontian Basin are from Gale et al. (2021) and Kennedy (2020). Sst—Sandstone; Mb—Member; R.—River; Cr.—Creek; GSSP—global stratotype section and point; Mari—*Mariella*; Ps.—*Pseudothalmanninella*; Th.—*Thalmanninella*; Pl.—*Planomalina*; Gr.—*Graysonites*; Ut.—*Utaturiceras*; Sto.—*Stoliczkaia*; Mant.—*Mantelliceras*; Pleur.—*Pleurohoplites*; tr—transitional morphotype; OAE1d—oceanic anoxic event 1d; Calc.—Calcareous; nanno—nannofossil; foram—foraminifera; Z—zone.

moto et al. (1999), Kawabe (2000), Obradovich et al. (2002), Matsumoto et al. (2003, 2004), and Kawabe et al. (2003).

C Isotope Stratigraphy of the Kyoei-Sakin-zawa, Hotei-zawa, and Penkemoyuparo River Sections

For C isotope analyses, wood fragments were removed from the same residue as planktic foraminifera and washed in methanol in an ultrasonic bath before immersion in 1 N HCl acid for 24 h. The wood fragments were then dried and crushed to powder. C isotopes in the acid-treated powdered wood samples were measured using a mass spectrometer (IsoPrime, GV Instruments) in line with an elemental analyzer (EuroEA3000, EuroVector) at the Tokyo University of Marine Science and Technology. Two specimens of each sample were measured, with C isotope ratios expressed as $\delta^{13}C_{wood}$ in ‰ units relative to the Vienna Peedee belemnite standard. The precision of the $\delta^{13}C$ measurements is ±0.1‰.

Os Isotope Stratigraphy of the Kyoei-Sakin-zawa Section

Determination of the water-column osmium isotope ($^{187}Os/^{188}Os$) composition at the time of sediment deposition was calculated from the rhenium-osmium (Re-Os) data of 43 samples of organic-bearing mudstone. Samples collected from outcrops were trimmed using a diamond saw blade with surfaces polished to remove cutting and drilling marks and eliminate any potential contamination. The samples were dried at 60 °C overnight and then were powdered in ceramic containers using high-purity crushing techniques at Tohoku University. The ceramic containers were cleaned using sand and washed and rinsed with ethanol. The powders were analyzed in the Durham Geochemistry Center at Durham University utilizing isotope dilution–negative ion mass spectrometry (Selby and Creaser, 2003; Cumming et al., 2013). In brief, sample powders (~1.0 g) were spiked with a mixed $^{185}Re + {}^{190}Os$ tracer solution and digested in sealed Carius tubes with 8 mL of 0.25 g/g CrO_3 in 4 N H_2SO_4 for ~48 h at 220 °C, principally leaching hydrogenous Re and Os from organic matter. The Os fraction was isolated and purified via chloroform extraction with back reduction into HBr and CrO_3·H_2SO_4-HBr microdistillation. The Re fraction was isolated via NaOH-acetone extraction and anion chromatography. Isotopic ratios of samples and solution standards (Re STD and DROsS) were

measured on a Thermo Scientific Triton thermal ionization mass spectrometer (TIMS) in negative ionization mode. Running average values for $^{187}Os/^{188}Os$ and $^{187}Re/^{185}Re$ solution standards to the time of these analyses (July 2024) were 0.16084 ± 0.00002 (1σ standard deviation [S.D.], $n = 1045$) and 0.59860 ± 0.00005 (1σ S.D., $n = 864$), respectively. Total procedural blanks were 9.9 ± 0.5 pg and 0.03 ± 0.00 pg (1σ S.D., $n = 8$) for Re and Os, respectively, with an average $^{187}Os/^{188}Os$ value of 0.20 ± 0.01 ($n = 8$). Present-day measured $^{187}Os/^{188}Os$ values of samples were corrected to initial $^{187}Os/^{188}Os$ values (Os_i) by accounting for postdepositional beta decay of ^{187}Re ($\lambda = 1.666 \times 10^{-11}$ yr^{-1}; Smoliar et al., 1996) using an age of 100.0 Ma.

$^{40}Ar/^{39}Ar$ Sanidine Dating

Sanidine was identified and separated from four tuffs, including HOT-002 (same as R8072 in Obradovich et al., 2002), Kiko-001, HgSm-001 (same as SK069 in Quidelleur et al., 2011), and R8943B (same as Obradovich et al., 2002). Stratigraphic context, biostratigraphic position, and location for each of these samples are summarized in Figure 2. Five additional tuffs from the Kyoei-Sakin-zawa section (Fig. 3) yielded no sanidine. Sanidine from the four tuffs was isolated using magnetic and gravity separation and identified using a scanning electron microscope as in Sageman et al. (2014). Sanidine separates were ultrasonically leached in 1.5 *M* HF for several minutes and rinsed repeatedly with deionized water prior to electron microscopy. The four sanidine separates were wrapped in aluminum foil, placed in one of 17 wells, each 4 mm in diameter by 4 mm deep in a 2.5-cm-diameter aluminum disk. Several crystals of the 28.201 ± 0.046 Ma Fish Canyon sanidine standard (Kuiper et al., 2008) were placed with the samples in each well. Irradiations were for 50 h in the cadmium-lined inner-core irradiation tube of the Oregon State University TRIGA reactor. The *J* values are based on single-crystal analyses of 12 Fish Canyon sanidine monitors collocated with samples in the irradiation disk.

Single-crystal fusion experiments at the University of Wisconsin–Madison WiscAr laboratory were undertaken with a 50 W CO_2 laser, followed by gas analysis in a Noblesse multicollector mass spectrometer as in Jicha et al. (2016). The isotopic composition of atmospheric argon used to calculate radiogenic argon percentages is from Lee et al. (2006). Ages were calculated using the decay constants of Min et al. (2000) and are reported as ± *X*/*Y*/*Z*, where *X* is the internal analytical uncertainty at the 95% confidence level, *Y* is this internal uncertainty plus that contributed by measurement of the *J* value, and *Z* is the total uncertainty, which includes the internal and *J* value uncertainties plus systematic contributions from uncertainty in the ^{40}K decay constant and age of the Fish Canyon sanidine standard. The total uncertainties were calculated using ArAR software (Mercer and Hodges, 2016).

U-Pb Zircon Dating

In total, 15 tuffs were collected from sections (summarized in Fig. 2) for U-Pb zircon chemical abrasion–isotope dilution–thermal ionization mass spectrometry (CA-ID-TIMS) dating at the Boise State University Isotope Geology Laboratory. Zircon crystals were placed in muffle furnaces at 900 °C for 60 h to anneal radiation-damaged domains (Mattinson, 2005). Individual crystals were mounted in epoxy, polished to center zones, and imaged by cathodoluminescence (CL). From the compiled images, spots were selected for laser ablation–inductively coupled plasma–mass spectrometry (LA-ICP-MS) using a Photon Machines Excite 193 nm excimer laser and Agilent 7700X quadrupole ICP-MS. Based on CL images and LA-ICP-MS data, single zircon grains were plucked from their respective

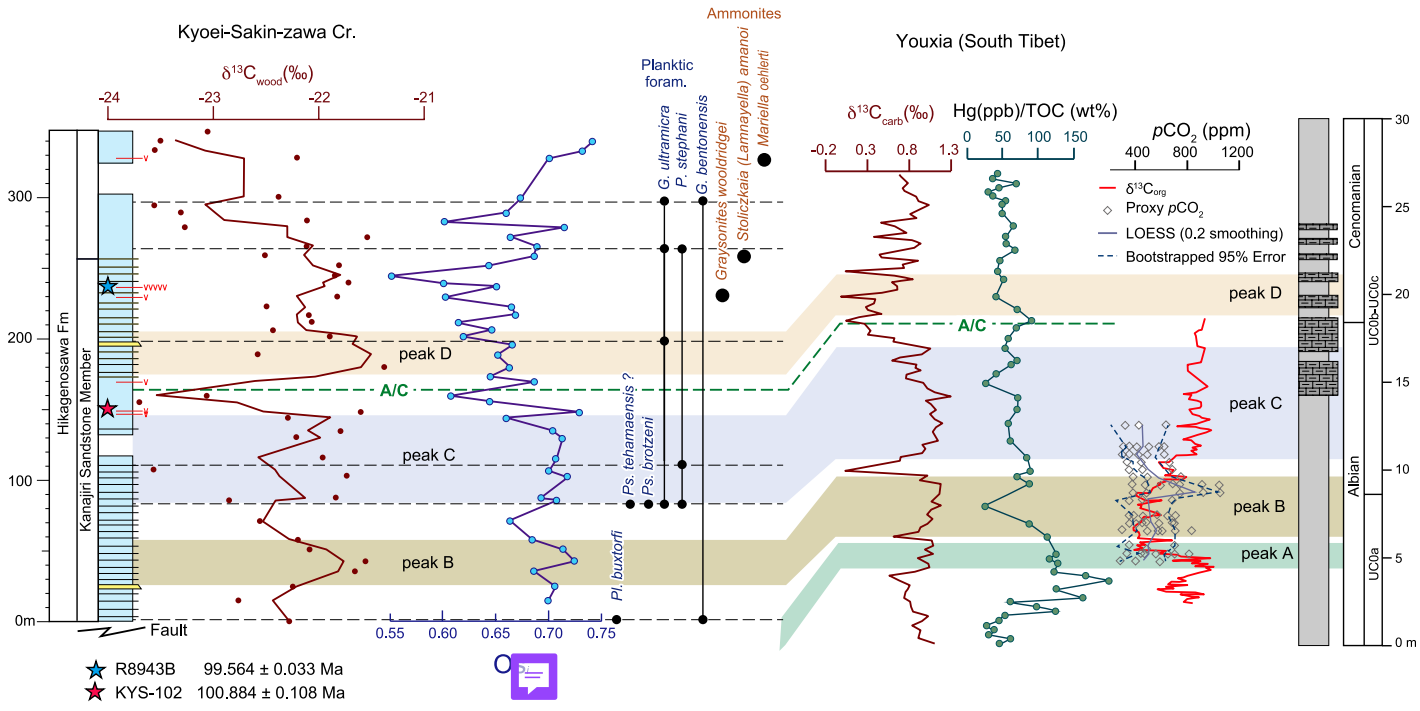

Figure 3. $\delta^{13}C_{wood}$ and Os_i isotope profiles with biostratigraphy of the Kyoei-Sakin-zawa section. The $^{206}Pb/^{238}U$ zircon ages of two tuffs (stars) are discussed in the main text; other tuffs are shown as red horizons with v. Brown profiles are three-point moving averages of the $\delta^{13}C$ values. Colored bands are correlation of positive C isotope excursions B, C, and D from the Youxia section (Yao et al., 2018, 2021) to those in the Kyoei-Sakin-zawa section. Stratigraphy legend is same as in Figure 2. A/C—Albian-Cenomanian boundary; TOC—total organic carbon; Cr.—Creek; *Ps.*—*Pseudothalmanninella*; *Pl.*—*Planomalina*.

epoxy mounts for the subsequent CA-ID-TIMS analysis. Individual zircon grains were chemically abraded in concentrated (29 *M*) HF at 190 °C for 12 h to mitigate open-system behavior and remove inclusions (Mattinson, 2005). The residual zircon grains were spiked with the EARTHTIME mixed ET535 or ET2535 tracer solution (Condon et al., 2015; McLean et al., 2015) and completely dissolved in 29 *M* HF at 220 °C for 48 h in Parr bombs. Following dissolution, the zircon + tracer solutions were dried to fluorides, and then redissolved in 6 *M* HCl at 180 °C overnight. Uranium and Pb were separated by anion-exchange column chromatography using 50 μL columns and AG-1 X8 resin (Krogh, 1973). The U and Pb isotopic measurements were performed on an IsotopX Phoenix X62 multicollector thermal ionization mass spectrometer. Determined U-Pb dates and uncertainties for each analysis were calculated from isotope ratio measurements using the algorithms of Schmitz and Schoene (2007) and the U decay constants of Jaffey et al. (1971).

RESULTS

Biostratigraphy and C Isotope Stratigraphy

Stratigraphically, the occurrences of planktic foraminifera are quite sporadic in each of the sections around the Albian-Cenomanian transition. Although the investigated sequences yield useful age-diagnostic species of planktic foraminifera, the abundance of these microfossils is very low, with only a few to several dozen individuals found in 400 g samples of mudstone. Preservation of foraminifera differ depending on the section. For example, in the Penkemoyuparo and Kotanbetsu River sections, preservation of foraminifera is moderate, whereas the Hotei-zawa and Kyoei-Sakin-zawa sections yield extremely well-preserved foraminifera (Fig. S2). We also note that "first occurrence" refers to the lowest stratigraphic finding of a given taxa within a specific level, whereas "first appearance" implies that is the first observed record of a given taxa's evolution. In Figure 2, we also make use of "occurrence" to simply indicate the observation of a given taxa in a location that likely does not represent the first or last occurrence in that section based on our stratigraphic correlations.

The Upper Albian index fossil *Planomalina buxtorfi* (Gandolfi, 1942) occurs in the basal parts of the Kyoei-Sakin-zawa and Penkemoyuparo River sections (Fig. 2). In the Kyoei-Sakin-zawa section, Upper Albian index fossil *Pseudothalmanninella ticinensis* (Sigal, 1948) also occurs from the base to middle parts of the Kanajiri Sandstone Member. *Thalmanninella brotzeni*, the first occurrence of which is uppermost Albian (Petrizzo et al., 2015), begins to occur in the lower to middle part of the Kanajiri Sandstone Member in the Hotei-zawa and Shumarinai River sections. *Thalmanninella globotruncanoides* is an important planktic foraminiferal species because the first occurrence is regarded as the primary marker for the base of the Cenomanian stage (Kennedy et al., 2004). In contrast with the strata in the GSSP, *Th. globotruncanoides* occurrences are extremely rare in the basal part of the Cenomanian in the Yezo Group. We found *Th. globotruncanoides* in the Penkemoyuparo, Kotanbetsu, and Shumarinai River sections, but we could not find this species in the Kyoei-Sakin-zawa and Hotei-zawa sections. The first appearance of *Th. globotruncanoides* is in the upper part of the Kanajiri Sandstone Member in the Shumarinai River section, whereas the first occurrence of this species is in the lower part of the Kanajiri Sandstone Member in the Penkemoyuparo River section (Fig. 2; Takashima et al., 2019). The occurrence of *Pseudothalmanninella tehamaensis* (Marianos and Zingaula) is regarded as a secondary criterion for placing the Abian-Cenomanian boundary (e.g., Kennedy et al., 2004; Petrizzo et al., 2015). The stratigraphic range of *Ps. tehamaensis*, including a transitional form from *Ps. ticinensis* to *Ps. tehamaensis*, is quite narrow, being restricted from the uppermost Albian to basal Cenomanian (Petrizzo et al., 2015). *Ps. tehamaensis* occurs in the Kanajiri Sandstone Member in the Kyoei-Sakin-zawa and Shumarinai and Penkemoyuparo River sections, where it co-occurs with *Th. brotzeni* and *Th. globotruncanoides* (Fig. 2). These lines of evidence suggest that the Albian-Cenomanian boundary occurs within the Kanajiri Sandstone Member. As for macrofossils, several important age-diagnostic species occur sporadically around the Albian-Cenomanian transition in the Hikagenosawa Formation. Upper Albian index fossils of *Pervinquieria (Subschloenbachia) rostrata* (Sowerby), *Pervinquieria subquadrata* Spath, and *Mariella bergeri* (Brongniart) have been reported from the lower part of the Hikagenosawa Formation (below the Kanajiri Sandstone Member) in the northern Tomamae and Oyubari areas, although they were not found in the sections investigated here (e.g., Matsumoto et al., 1999; Kawabe et al., 2003). Abundant early Cenomanian ammonites, such as *Graysonites wacoensis* Young (synonymous with *Graysonites wooldridgei* Young; Kennedy et al., 2005), *Mantelliceras saxbii* (Sharpe), *Mariella dorsetensis* (Spath), *Mariella oehlerti* (Pervinquière), *Utaturiceras vicinale* (Stoliczka), and *Stoliczkaia* (*Lamnayella*) cf. *amanoi* Matsumoto and Inoma, have been reported from the middle to upper part of the Kanajiri Sandstone Member in the sections investigated here (Fig. 3; Matsumoto et al., 1999, 2003; Obradovich et al., 2002). Although *G. wacoensis* occurs below the Kanajiri Sandstone Member in the Hotei-zawa section, the horizon is truncated by faults, so the stratigraphic position of this fossil occurrence is not clear. These early Cenomanian ammonites occur at higher levels than those of *Planomalina buxtorfi* and *Ps. ticinensis*, and their stratigraphic occurrences are consistent with those of the planktic foraminifera (Fig. 3).

The $\delta^{13}C_{wood}$ values range between −25.9‰ and −20.6‰ (Table S1). Since there is a pronounced sample-to-sample variation in the $\delta^{13}C_{wood}$ value, a three-point moving average is shown as the curves in Figures 2 and 3. The variability between $\delta^{13}C_{wood}$ values is inherently greater than that of the $\delta^{13}C_{carbonate}$ pool, which produces some differences between the $\delta^{13}C_{wood}$ profiles and the $\delta^{13}C_{carbonate}$ record from the Vocontian Basin (Fig. 2). Notwithstanding this variability, our dataset is robust enough to allow for confident correlation between these records by augmenting the C isotope chemostratigraphy with biostratigraphic and radioisotopic constraints. The strata around the Kanajiri Sandstone Member are characterized by a broad positive peak consisting of several smaller peaks in the $\delta^{13}C_{wood}$ curve in each of the five sections (Fig. 2).

Os Isotope Stratigraphy

The Re and Os abundances for the sample set are similar throughout the section (0.3–1.1 ppb and 30–62 ppt, respectively), with calculated Os_i values ranging from 0.55 to 0.74 (Table S2). From the base of the section upward to ~145 m, Os_i values are relatively similar, averaging ~0.7. However, the overall similarity in Os_i values is interrupted by a trend to an Os_i value of ~0.66 between ~46 m and 71 m, which occurs within peak B and before peak C of the C isotope profile. A progressive shift toward less radiogenic values over 110 m to a nadir of 0.55 occurs between ~134 m and 245 m (Fig. 3). The start of the shift toward less radiogenic Os_i values coincides with a prominent negative shift in the $\delta^{13}C_{wood}$ values at the Albian-Cenomanian boundary that occurs between 140 m and 160 m (Fig. 3). At ~260 m in the section, the Os_i values progressively return toward more radiogenic compositions, with values reaching a maximum of 0.74 in the uppermost part of the section.

U-Pb Zircon and $^{40}Ar/^{39}Ar$ Sanidine Chronology

We report weighted mean ages from 10 tuffs (see Table 1; complete isotopic data in Table S3) based on the youngest $^{206}Pb/^{238}U$ dates that meet

TABLE 1. SUMMARY OF RADIOISOTOPIC AGES FROM TUFFS OF THE ALBIAN-CENOMANIAN BOUNDARY SECTIONS, HOKKAIDO, JAPAN: $^{206}Pb/^{238}U$ RESULTS, TOMAMAE AND OYUBARI AREAS

Tuff sample	Height above base of section (m)	Latitude (°N)	Longitude (°E)	*N*	MSWD	Weighted mean age (Ma)	$\pm 2\sigma_{int}$	$\pm 2\sigma_{tr}$	$\pm 2\sigma_{tot}$
Tomamae area									
HOT-002	325	44.27220	142.08588	3/6	1.59	99.311	0.051	0.06	0.12
HOT-003	310	44.27198	142.08633	2/6	4.83	99.563	0.347	0.35	0.36
HOT-004	246	44.27258	142.08698	6/12	1.25	99.644	0.021	0.04	0.11
Hiko-001	293	44.19023	142.06255	3/5	1.25	98.914	0.054	0.06	0.12
SK069	242	44.27997	142.08236	6/9	1.43	99.695	0.019	0.04	0.11
R8943B	None	44.26097	142.09273	5/7	0.23	99.564	0.033	0.04	0.12
Oyubari area									
PeHi-014	520	43.10882	142.18240	3/9	0.41	98.821	0.052	0.06	0.12
PeHi-013	471	43.10933	142.18287	4/6	0.71	98.968	0.032	0.04	0.11
PeHi-012	448	43.10908	142.18325	7/10	0.97	98.991	0.022	0.04	0.11
PeHi-011	428	43.10897	142.18345	2/10	0.52	99.525	0.159	0.16	0.19

Note: *N*—number of single-crystal dates used for age calculation relative to the total number of dates; MSWD—mean square of weighted deviates; $\pm 2\sigma_{int}$—analytical uncertainty only at the 95% confidence interval; $\pm 2\sigma_{tr}$—analytical plus tracer uncertainty; $\pm 2\sigma_{tot}$—fully propagated uncertainty at the 95% confidence interval including analytical, tracer/standard age, and decay constant uncertainties.

the modified Thompson tau outlier rejection criteria ($p = 0.05$; Thompson, 1935). Individual zircon dates that are older than the youngest statistical group are interpreted to reflect magmatic antecrysts or epiclastic inheritance. Of the 5–12 zircons measured from each tuff, one to six zircons were found to be inherited (Fig. 4). Three tuffs contained four crystals between them that were younger than the statistically youngest group; these are interpreted to have lost radiogenic Pb (^{206}Pb) and were thus excluded from the weighted mean age calculation (Fig. 4). Zircon separation was attempted from five additional ash beds in the Kyoei-Sakin-zawa section. Three of these contained no zircon (KYS-101, KYS-103, KYS-106), and although KYS-104 contained zircon, it was collected only 8 m below R8943B and would likely not be distinguishable from the latter data, so these zircons were not measured. Six zircon crystals from 2-cm-thick tuff KYS-102 yielded highly dispersed dates ranging from 135.193 ± 0.075 Ma to 100.884 ± 0.108 Ma (Table S4). With caution, we use the youngest date as a minimum depositional age for this horizon in the Kyoei-Sakin-zawa section (Figs. 3 and 4).

For four of the tuffs for which $^{206}Pb/^{238}U$ dates are reported, we report also weighted mean ages in Table 2 based on the youngest $^{40}Ar/^{39}Ar$ dates that yielded an MSWD value below the critical value (Schaen et al., 2021, method 1). No other tuffs from the Kyoei-Sakin-zawa section were found to contain sanidine. From the four that contained sanidine, individual dates that are older than the youngest group are interpreted to reflect inheritance of magmatic antecrysts, or, more likely in this forearc depositional setting, these are reworked epiclastic crystals. Two of the tuffs, Hiko-001 and HOT-002, contained little or no inherited sanidine crystals, whereas in two others, SK069 and R8943B, 48% and 68%, respectively, of the crystals are interpreted to reflect inheritance of older crystals into the deposits (Fig. 4). The complete $^{40}Ar/^{39}Ar$ isotopic dataset is given in Table S4. Three tuffs, Hiko-001, SK069, and R8943B, yielded $^{206}Pb/^{238}U$ and $^{40}Ar/^{39}Ar$ dates that are indistinguishable from one another. In contrast, tuff HOT-002 yielded a $^{206}Pb/^{238}U$ date of 99.311 ± 0.051/0.06/0.12 Ma, which is significantly younger than the $^{40}Ar/^{39}Ar$ date of 99.853 ± 0.040/0.04/0.16 Ma. We are unable to explain the cause of this disagreement but note that the $^{206}Pb/^{238}U$ date overlaps with the age for this tuff reported by Obradovich et al. (2002; cf. Fig. 4 here), so we exclude these $^{40}Ar/^{39}Ar$ data from further discussion.

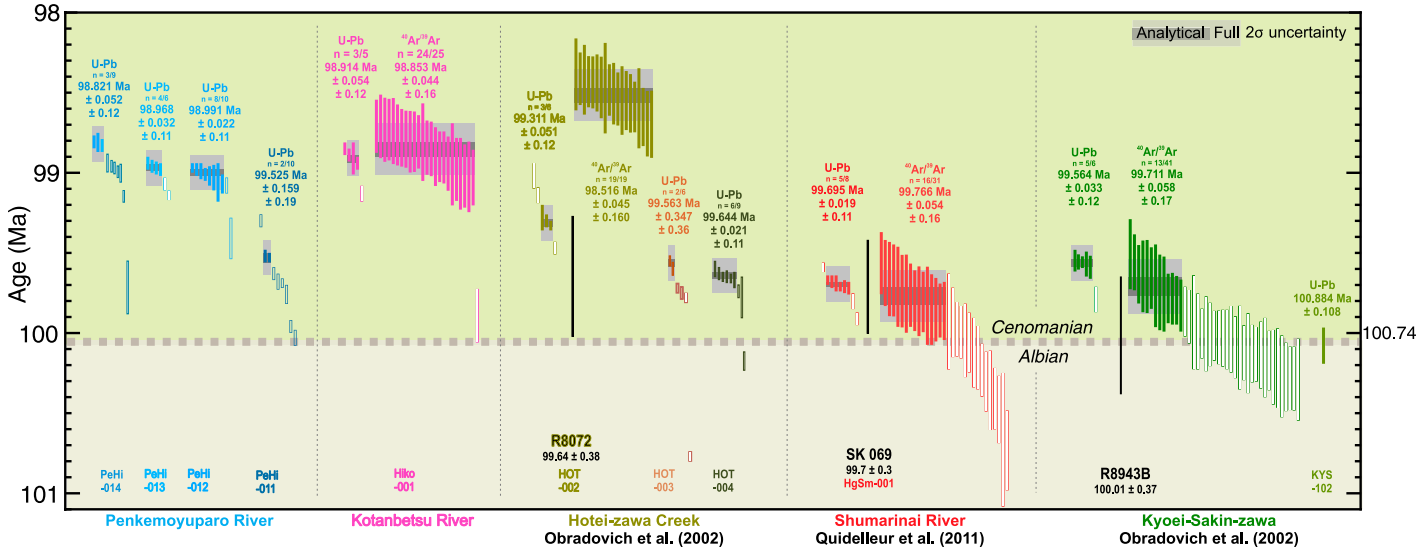

Figure 4. Rank order plot of $^{206}Pb/^{238}U$ zircon and $^{40}Ar/^{39}Ar$ sanidine dates from 11 tuffs. For each tuff, individual symbols are dates from single crystals with the weighted mean ages and uncertainties shown. Unfilled dates were excluded from the weighted mean age calculation. Only the youngest zircon from tuff KYS-102 in the Kyoei-Sakin-zawa section is shown.

TABLE 2. SUMMARY OF RADIOISOTOPIC AGES FROM TUFFS OF THE ALBIAN-CENOMANIAN BOUNDARY SECTIONS, HOKKAIDO, JAPAN: $^{40}Ar/^{39}Ar$ RESULTS, TOMAMAE AREA

Tuff sample	Height above base of section (m)	Latitude (°N)	Longitude (°E)	*N*	MSWD	Weighted mean age (Ma)	$\pm 2\sigma_{int}$	$\pm 2\sigma_{int+J}$	$\pm 2\sigma_{tot}$
HOT-002	325	44.27220	142.08588	19/19	0.96	98.516	0.045	0.05	0.16
Hiko-001	293	44.19023	142.06255	24/25	1.22	98.853	0.044	0.04	0.16
SK069	242	44.27997	142.08236	16/31	0.83	99.766	0.054	0.05	0.16
R8943B	None	44.26097	142.09273	13/41	1.13	99.711	0.058	0.06	0.17

Note: Ages relative to Fish Canyon sanidine interlaboratory standard at 28.201 Ma (Kuiper et al., 2008); decay constant after Min et al. (2000). *N*—number of single-crystal dates used for age calculation relative to the total number of dates; MSWD—mean square of weighted deviates; $\pm 2\sigma_{int}$—analytical uncertainty only at the 95% confidence interval; $\pm 2\sigma_{int+J}$—analytical uncertainty at the 95% confidence interval including *J* uncertainty; $\pm 2\sigma_{tot}$—fully propagated uncertainty at the 95% confidence interval including analytical, tracer/standard age, and decay constant uncertainties.

DISCUSSION

Biostratigraphy and C Isotope Correlation

The GSSP for the base of the Cenomanian stage is defined at a level 36 m below the top of the Marnes Bleues Formation, a level that corresponds to the first appearance of the planktic foraminifera *Thalmanninella globotruncanoides* (= *Rotalipora globotruncanoides* Sigal, 1948), on the south side of Mont Risou, southeast France (Kennedy et al., 2004). The $\delta^{13}C$ profile around the Albian-Cenomanian transition at the GSSP is characterized by the broad positive peak of the Albian-Cenomanian boundary event, which is subdivided into four subordinate positive peaks A through D. The base of Cenomanian at the GSSP also corresponds to the trough in the $\delta^{13}C$ curve between peaks C and D (Fig. 2). At the GSSP section, detailed macrofossil and microfossil biostratigraphy reveals several bioevents associated with the Albian-Cenomanian boundary event interval (Gale et al., 1996; Kennedy et al., 2004; Gale et al., 2011; Petrizzo et al., 2015).

As for the Yezo Group, the Albian-Cenomanian boundary has been presumed to occur within the Kanajiri Sandstone Member of the Hikagenosawa Formation based mainly on macrofossil and microfossil biostratigraphy (Matsumoto et al., 1999, 2000; Kawabe et al., 2003). However, the absence of the important age-diagnostic ammonite *Mantelliceras mantelli* as well as sporadic and rare occurrences of the planktic foraminifera *Th. globotruncanoides* make it challenging to identify the exact horizon of the Albian-Cenomanian boundary. Takashima et al. (2019) determined the detailed stratigraphic position of the Albian-Cenomanian boundary within the upper part of the Kanajiri Sandstone Member of the Yezo Group in the Shumarinai River section based on C isotope stratigraphy and planktic foraminiferal biostratigraphy. The Albian-Cenomanian boundary horizon in the Shumarinai River section is characterized by first appearance of *Th. globotruncanoides* and by a negative trough in the $\delta^{13}C$ profile between two positive peaks, which are correlated with peaks C and D of the GSSP, respectively (Fig. 2). Although Cenomanian index fossils occur in this section, no age-diagnostic fossils have been obtained from this interval that can be identified as Albian.

The C isotope and planktic foraminiferal biostratigraphy presented here associated with the Kanajiri Sandstone Member in the Hotei-zawa, Kyoei-Sakin-zawa, and Penkemoyuparo River sections allows us to reexamine the validity of the correlation by Takashima et al. (2019). An updated interregional and international correlation around the Albian-Cenomanian transition is presented in Figure 2. This correlation is based on macrofossil and microfossil occurrences and radioisotopic ages, as well as matching of $\delta^{13}C$ profiles.

In the Penkemoyuparo River section, a faint positive peak in $\delta^{13}C$ is identified in the taxon range zone of *Planomalina buxtorfi*, which is an Upper Albian index fossil. Such a $\delta^{13}C$ peak is biostratigraphically restricted to peak A at the GSSP (Fig. 2). In the Kyoei-Sakin-zawa and Penkemoyuparo River sections, a positive peak in $\delta^{13}C$ occurs just above the last occurrence of *Pl. buxtorfi*. The uppermost Albian index ammonite fossil *Mariella bergeri* has been reported from the corresponding stratigraphic level near the Penkemoyuparo River section in the Oyubari area (Matsumoto et al., 1999; Kawabe et al., 2003). Considering the biostratigraphic evidence, this $\delta^{13}C$ peak can be correlated with peak B of the GSSP (Fig. 2). Strata in peak C of the GSSP are associated with the first occurrence of *Th. brotzeni* and the last occurrences of *Ps. ticinensis* and *Mariella bergeri*. The correlative positive $\delta^{13}C$ peak corresponds with strata that contain the last occurrence of *Ps. ticinensis* and the occurrence of *Th. brotzeni* in the Kyoei-Sakin-zawa and Hotei-zawa sections, respectively. On the other hand, the basal Cenomanian ammonite *Gr. wacoensis* occurs at the base of the interval where we have placed peak C in the Hotei-zawa section. However, the outcrop that yielded the *Gr. wacoensis* fossil is adjacent to a major fault (Fig. 1). Given the poor outcrop exposure between 110 m and 210 m (Fig. 2), we cannot rule out that the lower part of the Hotei-zawa section is repeated owing to displacement on an undetected fault. Therefore, the stratigraphic position of *Gr. wacoensis* in the Hotei-zawa section is not certain, and we cannot correlate peak C from the GSSP with confidence (Fig. 2). A sharp negative $\delta^{13}C$ excursion just above peak C was identified in the Shumarinai River and Kyoei-Sakin-zawa sections. This negative $\delta^{13}C$ excursion is correlated with the base of the Cenomanian because *Th. globotruncanoides* and *Ps. tehamaensis* occur at this horizon (Takashima et al., 2019). The corresponding excursion in the $\delta^{13}C$ profiles is also seen in the Hotei-zawa section (Fig. 2). The overlying positive peak, correlated with peak D of the GSSP, can be identified in each of the five Yezo Group sections, although the variance in the $\delta^{13}C_{wood}$ values, for example, in the Hotei-zawa section, introduces some uncertainty. In the Penkemoyuparo River section, the first occurrences of *Th. globotruncanoide*s and *Ps. tehamaensis* (317.1 m) are identified in this peak. Considering the long stratigraphic barren zone of planktic foraminifera in this section, the Albian-Cenomanian boundary can be placed below this horizon (Fig. 2). Diversified Cenomanian ammonites, including *Gr. wacoensis*, *Utaturiceras vicinale (Stoliczka)*, *Mariella oehlerti*, and *Mantelliceras saxbii* Sharpe, begin to occur within this horizon (Figs. 2 and 3).

Origin of the Transition Toward Less Radiogenic Os_i

In the Kyoei-Sakin-zawa section, the onset of a progressive shift to less radiogenic Os_i values corresponds with the prominent negative $\delta^{13}C_{wood}$ excursion that occurs within the Albian-Cenomanian boundary interval between peaks C and D of the Albian-Cenomanian boundary event (Fig. 3). This shift to less radiogenic Os_i values is not accompanied by the kind of orders-of-magnitude increase in common Os concentration (typically shown by ^{192}Os abundance) that is observed with OAE1a and OAE2 (e.g., Tejada et al., 2009; Li et al., 2024; Jones et al., 2023; Takashima et al., 2024; see also Table S3).

Osmium isotope stratigraphy for two other basins (Umbria-March basin [Bottaccione and

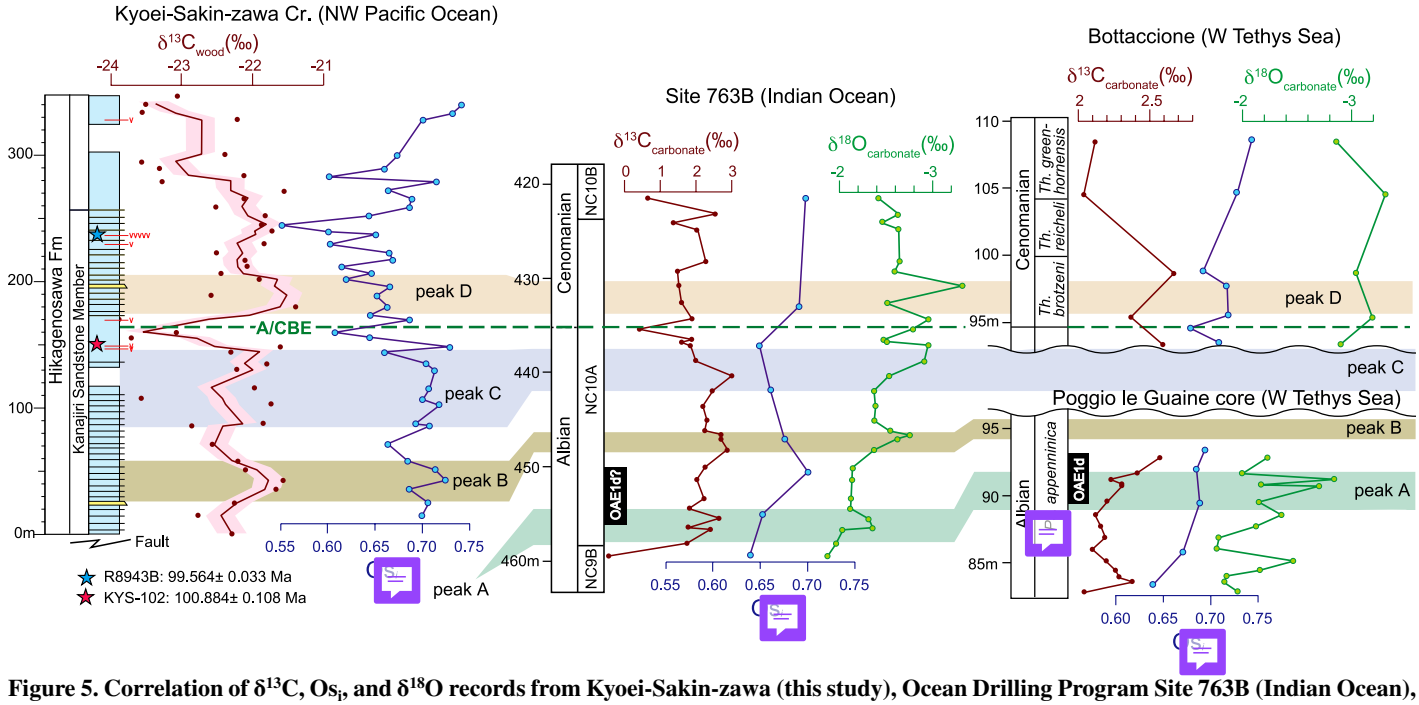

Figure 5. Correlation of $\delta^{13}C$, Os_i, and $\delta^{18}O$ records from Kyoei-Sakin-zawa (this study), Ocean Drilling Program Site 763B (Indian Ocean), and Bottaccione and Poggio le Guaine, Italy (Matsumoto et al., 2022). The $^{206}Pb/^{238}U$ zircon ages of two tuffs marked with stars are discussed in the text. A/CBE—Albian-Cenomanian boundary event; Cr.—Creek; OAE1d—oceanic anoxic event 1d; Ps.—*Pseudothalmanninella*; Th.—*Thalmanninella*.

Poggio le Guaine] and Ocean Drilling Program [ODP] Site 763B [Indian Ocean]; Matsumoto et al., 2022) is of low resolution and/or absent from entire intervals or parts of the Albian-Cenomanian boundary event carbon isotope profile. Thus, a site-to-site comparison is severely hampered, particularly with the high-resolution Os_i record for the Kyoei-Sakin-zawa section (Fig. 5). Although the Os_i values for both the Umbria-March Basin and Indian Ocean have low resolution, broad trends can be compared to the Kyoei-Sakin-zawa section. For the Umbria-March Basin, the available Os_i data show a decrease in the Os_i value from ~0.70 to ~0.67 at the Albian-Cenomanian boundary and then a return to more radiogenic Os_i values up section, above peak D, similar to the Kyoei-Sakin-zawa section (Fig. 5). Although lacking resolution, the Os_i values for the Indian Ocean (ODP Site 763B) trend to less radiogenic values toward/across the Albian-Cenomanian boundary and then broadly trend toward more radiogenic Os_i values up section (Fig. 5).

Unlike OAE1a, the Wezel Level, Fallot Level, and OAE2, which each show a prominent shift to less radiogenic Os_i associated with an abrupt negative $\delta^{13}C$ excursion, the OAE1c and OAE1d intervals are characterized by more subdued $\delta^{13}C$ excursions and are not associated with extreme shifts in Os_i (Matsumoto et al., 2022). In fact, OAE1d Os_i data, while of low resolution, for the Indian Ocean (763B) and Umbria-March Basin (Bottaccione and Poggio le Guaine) are very similar (~0.65–0.68; Fig. 5; Matsumoto et al., 2022).

Here, we examine various hypotheses that might explain the subdued shift toward less radiogenic Os_i observed in the Yezo Group during the Albian-Cenomanian boundary event and Os_i features of OAE1d relative to other mid-Cretaceous OAEs. These include (1) injection of a lower quantity of less radiogenic Os into the oceans owing to limited volcanic and hydrothermal activity within large igneous provinces; (2) deposition of the Yezo Group in a restricted basin that was insulated from effects of large igneous province activity on seawater, (3) surface weathering of less radiogenic basaltic rocks, rather than radiogenic continental igneous and metamorphic rocks; (4) increased mid-ocean-ridge volcanism; and (5) atmospheric and sea-surface cooling associated with a sea-level fall that modulated delivery of radiogenic Os to the ocean.

With regard to hypothesis 1: Limited $^{40}Ar/^{39}Ar$ dates of submarine basalts and geophysical models of crustal volumes imply that a short-lived order-of-magnitude increase to a peak magma flux of 0.9 km^3/yr occurred within the central Kerguelen Plateau and Broken Ridge large igneous province ca. 100 Ma, spanning the Albian-Cenomanian boundary event period and including OAE1d (Coffin et al., 2002; Duncan, 2002; Jiang et al., 2021). This elevated large igneous province activity at ca. 100 Ma is thus a probable source of less radiogenic Os, but it is unclear why the shift in Os_i values in the Yezo Group is not as prominent as, for example, that during OAE1a (Li et al., 2024) or OAE2 (Du Vivier et al., 2015; Takashima et al., 2024). Moreover, the low and similar concentrations of ^{192}Os (between 11 ppt and 24 ppt) throughout the Kyoei-Sakin-zawa section (Table S3) suggest that the contribution of large igneous province–derived Os could have been limited. At Site 763B and Bottaccione, lesser shifts toward unradiogenic Os_i through the interval comprising C isotope peaks B through D are accompanied by weakly decreasing $\delta^{18}O_{carbonate}$ values, suggesting ocean warming and perhaps increasing continental weathering during this period (Fig. 5; Matsumoto et al., 2022). An increase in mercury concentration associated with an increase in $\Delta^{199}Hg$ in sediments just prior to the onset of the Albian-Cenomanian boundary event interval [illegible]x $\Delta^{199}Hg$ and Hg/total organic carbon [illegible]values preceding peak A; Fig. 3) within the Youxia section, Tibet, was interpreted to reflect volcanic input from a subaerial phase of the peak activity in the Kerguelen Plateau large igneous province (Yao et al., 2021). Our correlation between records from Hokkaido and Tibet suggests that the mercury increase occurred imme-

diately prior to positive $\delta^{13}C$ peak A, several hundred thousand years before the shift in Os_i values, which is, unfortunately, not recorded at Kyoei-Sakin-zawa (Fig. 3). In the Youxia section, Hg/TOC decreases while proxy pCO_2 increases within the positive C isotope excursion of peak B (Fig. 3; Yao et al., 2021), features that coincide with a trend to decreasing Os_i in the Kyoei-Sakin-zawa section. Taken together, these observations are difficult to reconcile with a mainly volcanic driver for OAE1d or the Albian-Cenomanian boundary event.

Regarding hypothesis 2: The Yezo Group was deposited in a Pacific Ocean–facing basin (Itoh et al., 2017), implying that the sediments should reflect the global, not regional, seawater osmium isotope composition. Considering hypothesis 3, it is possible that weathering of relatively large areas of subaerially erupted basalt that formed the Kerguelen Plateau (Frey et al., 2003) may have supplied unradiogenic Os to the ocean. In this scenario, the effects on seawater Os might have been similar to those of a low level of submarine volcanism and hydrothermal activity associated with the Kerguelen Plateau, as has been proposed for erosion of the Deccan Traps prior to the Cretaceous-Paleogene boundary (Westerhold et al., 2025). There is simply little, if any, evidence in favor of an enhanced spreading rate along the mid-ocean-ridge system during the Albian-Cenomanian boundary event and OAE1d periods, ruling out hypothesis 4.

The deposition of turbidite-produced sandstone beds beginning in the late Albian and becoming prominent during the early Cenomanian, including the Kanajiri Sandstone Member of the Hikagenosawa Formation (Fig. 2), marks a relatively abrupt change from mudstone sedimentation that may be interpreted as a regional sequence boundary reflecting a sea-level fall. Indeed, the timing of this shift in sedimentation in the Yezo Group around the Albian-Cenomanian boundary corresponds with a prominent sequence boundary that reflects a global eustatic fall in sea level known as KAl8 (Haq, 2014). Moreover, based on a positive shift in $\delta^{18}O$ values and microfossil occurrences in sediment from Blake Nose in the North Atlantic Ocean, an abrupt decrease in global sea-surface temperature by ~3 °C is inferred that begins following the Albian-Cenomanian boundary (Wilson and Norris, 2001). Thus, hypothesis 5—abrupt cooling of the atmosphere and sea-surface temperature accompanying a fall in sea level—may have played a role in modulating the seawater Os_i values. If the contribution of Os to seawater from a large igneous province source remained constant, for example, during the peak of Kerguelen Plateau eruptive activity, a decrease in continental weathering could have sufficiently suppressed the delivery of radiogenic Os to the ocean to impart a decline in seawater $^{187}Os/^{188}Os$. This is true whether the source of unradiogenic Os was submarine in origin or derived from subaerial weathering of Kerguelen Plateau basalt (hypothesis 4, previously mentioned). A return of atmospheric and sea-surface temperatures to levels preceding OAE1d and the Albian-Cenomanian boundary event would have increased weathering and delivery of radiogenic Os to the ocean, thereby diluting the waning contribution of Os from large igneous province volcanism. A less prominent sea-level fall tentatively known as KCe1 occurred during the early Cenomanian prior to the first occurrence of *Mantelliceras saxbii* (Haq, 2014) and could have been responsible for the short-lived shift to unradiogenic Os_i at 280 m in the Kyoei-Sakin-zawa section (Fig. 3). In contrast, neither OAE1a nor OAE2—each associated with abrupt shifts to much less radiogenic seawater Os_i ratios of 0.2 or lower with enrichment in ^{192}Os abundance—coincided with a lowering of sea-surface temperature or a major global eustatic fall in sea level (Haq, 2014).

Chronostratigraphy of the Albian-Cenomanian Boundary

Three tuffs, each in a different stratigraphic section, yielded $^{40}Ar/^{39}Ar$ and $^{206}Pb/^{238}U$ ages that are not distinguishable from one another when the total uncertainties are considered. Notwithstanding this uncertainty, the level of inheritance in tuff R8943B revealed in our single sanidine dates suggests the age determined by Obradovich et al. (2002) for this tuff, based on six aliquots of between two and four crystals each, may have masked these older crystals, thereby biasing the result toward an older age. Similarly, tuff SK069 shows a high level of inherited sanidine crystals (Fig. 4). Because these are among the tuffs critical for dating the base of the Cenomanian, given the degree of inheritance, we instead prefer the more precise $^{206}Pb/^{238}U$ ages. The oldest $^{206}Pb/^{238}U$ ages of 99.644 ± 0.016 Ma, 99.695 ± 0.015 Ma, and 99.564 ± 0.033 Ma are from the Hotei-zawa, Shumarinai River, and Kyoei-Sakin-zawa sections, respectively. In the Kyoei-Sakin-zawa section, there is the additional $^{206}Pb/^{238}U$ age of 100.884 ± 0.108 Ma from the single youngest zircon. An 88 m section of mudstone separates the latter tuff from R8943B, dated at 99.564 ± 0.033 Ma (Fig. 3), which, assuming a constant sedimentation rate, implies deposition at 0.067 m/k.y. Using this sedimentation rate and extrapolating to 160 m above the base of this section yields an age for the Albian-Cenomanian boundary of 100.74 ± 0.10 Ma. Assuming a 10% uncertainty in the mean sedimentation rate translates into an uncertainty of ~30 k.y. on the boundary age. We thus propose an age for the Albian-Cenomanian boundary of 100.74 ± 0.10 Ma, which includes the uncertainty on the lone Albian date (Figs. 3 and 4). Placing the Albian-Cenomanian boundary at 100.74 ± 0.10 Ma compares well with age estimates of this boundary based on chronostratigraphic analysis of flooding events in the Texas Gulf Coast and Western Interior Basin (Scott et al., 2018).

Singer et al. (2021, 2025) proposed an age for the Albian-Cenomanian boundary of 100.00 ± 0.40 Ma that relied on a $^{40}Ar/^{39}Ar$ age of 100.07 ± 0.07 Ma from a bentonite at the base of the early Cenomanian Shell Creek Shale in the Western Interior Basin, coupled with the (recalibrated) age of 100.01 ± 0.37 Ma obtained by Obradovich et al. (2002) from tuff R8943B in the Kyoei-Sakin-zawa section, Hokkaido, Japan. The age we propose here, 100.74 ± 0.10 Ma, is significantly older than the estimate of Singer et al. (2021, 2025) and more precise by a factor of four. Importantly, unlike radioisotopic estimates from the Western Interior Basin, the Albian-Cenomanian age proposed here is supported by microfossil and macrofossil biostratigraphy and C isotope correlation with the GSSP section in France. In turn, considering the age of the Aptian-Albian boundary at 113.2 ± 0.30 Ma (Selby et al., 2009; Gale et al., 2020), the duration of the Albian stage becomes 12.46 ± 0.30 m.y., nominally shorter than the 12.7 m.y. in GTS2020 and with an uncertainty based on bracketing radioisotopic age determinations.

Our findings bear on the veracity of orbital age models acquired from Albian sediments. For example, Grippo et al. (2004) inferred 29 long eccentricity cycles—each of 406 k.y. duration—comprising the Albian stage in the Piobbico core, Italy, implying a duration of 11.8 ± 0.40 m.y. Gale et al. (2011) correlated these findings from the Piobbico core to the section at Col de Palluel/Mont Risou, France, and via orbital tuning of whole-rock Al_2O_3 contents concluded that the duration of the Albian stage was 10.64 m.y. Our findings imply that several long eccentricity cycles are either missing, poorly expressed, or misidentified in these Tethyan successions.

CONCLUSIONS

Radioisotopic dating of tuffs in early Cenomanian strata of Hokkaido, Japan, supports an age for the base of the Cenomanian stage—and thus for the Albian-Cenomanian boundary—of 100.74 ± 0.10 Ma. Moreover, radioisotopic dating indicates that the duration of the Albian stage was 12.46 ± 0.30 m.y.

This duration is much longer than estimates based on cyclostratigraphy and orbital tuning of the Piobbico core, Italy (11.8 m.y.; Grippo et al., 2004), or the section at Col de Palluel/ Mont Risou, France (10.64 m.y.; Gale et al., 2011). Based on radioisotopic dating, 31 long eccentricity cycles of 405 k.y. duration transpired during the Albian stage. Future work is required to understand why the astronomical age models from these Tethyan records underestimate the duration of the Albian stage by 600 k.y. or more.

The C and Os isotope profiles alongside the macrofossil and microfossil occurrences and radioisotope-based age model of the Kyoei-Sakin-zawa section together provide a new stratigraphic framework for correlating the Albian-Cenomanian boundary interval to other sections and marine cores as more Os isotope data are collected. The initiation of a modest shift toward less radiogenic Os_i values during the final ~100,000 yr of the Albian suggests that the Albian-Cenomanian boundary event, including the sharp negative $\delta^{13}C$ excursion demarcating the Albian-Cenomanian boundary, was coeval with volcanic activity associated with the peak eruptive phase of the Kerguelen Plateau at ca. 100 Ma. Proxy records of a global drop in sea-surface, and thus atmospheric, temperature at this same time are associated with a prominent sequence boundary and global fall in sea level. If large igneous province volcanism was responsible for lowering Os_i values, then the modest shift observed may reflect suppression of continental weathering and reduced delivery of radiogenic Os to the ocean during relatively cool surface conditions. To gain a more complete understanding of drivers of OAE1d and the Albian-Cenomanian boundary event and to further test our hypothesis, additional high-resolution records of Os and Hg concentrations and isotope ratios from sediments spanning the Albian-Cenomanian boundary will be required. In parallel, improvement of the precision and accuracy of the chronology of Kerguelen Plateau volcanism remains key to understanding what role it played in generating OAE1d and the Albian-Cenomanian boundary event.

ACKNOWLEDGMENTS

John Obradovich and Bill Cobban inspired and supported this research in its earliest stages. Conversations with David Sawyer over many years kept this effort moving forward and are much appreciated. We thank Jim Crowley for assistance with U-Pb analytical work, and Bryan Wathen and Alec Baudry for extraction of zircon from tuffs. Chris Ottley and Geoff Nowell are acknowledged for laboratory support. This work was supported by U.S. National Science Foundation grants EAR-1951812 (B.S. Singer), EAR-1952346 (M.D. Schmitz), and EAR-1951835 (B.B. Sageman), U.K. Natural Environment Research Council grant NE/V019406/1 (D. Selby), and Japan Science Foundation grants KAKENHI 21H04503 and 18KK0091 (R. Takashima). B.S. Singer is grateful for a fellowship from the Japan Society for the Promotion of Science during the preparation of this work.

REFERENCES CITED

Bornemann, A., Pross, J., Reichelt, R., Herrle, J.O., Hemleben, C.G., and Mutterlose, J., 2005, Reconstruction of short-term paleoceanographic changes during the formation of the late Albian 'Niveau Breistroffer' black shales (oceanic anoxic event 1d, SE France): Journal of the Geological Society, v. 162, https://doi.org/10.1144/0016-764903-171.

Cobban, W.A., Walaszczyk, I., Obradovich, J.D., and McKinney, K.C., 2006, A USGS Zonal Table for the Upper Cretaceous Middle Cenomanian–Maastrichtian of the Western Interior of the United States Based on Ammonites, Inoceramids, and Radiometric Ages: U.S. Geological Survey Open-File Report 2006-1250, 45 p., https://doi.org/10.3133/ofr20061250.

Coffin, M.F., Pringle, M.S., Duncan, R.A., Gladczenko, T.P., Storey, M., Müller, R.D., and Gahagan, L.A., 2002, Kerguelen hotspot magma output since 130 Ma: Journal of Petrology, v. 43, p. 1121–1137, https://doi.org/10.1093/petrology/43.7.1121.

Condon, D.J., Schoene, B., McLean, N.M., Bowring, S.A., and Parrish, R.R., 2015, Metrology and traceability of U-Pb isotope dilution geochronology (EARTHTIME tracer calibration part I): Geochimica et Cosmochimica Acta, v. 164, p. 464–480, https://doi.org/10.1016/j.gca.2015.05.026.

Cumming, V.M., Poulton, S.W., Rooney, A.D., and Selby, D., 2013, Anoxia in the terrestrial environment during the late Mesoproterozoic: Geology, v. 41, p. 583–586, https://doi.org/10.1130/G34299.1.

Duncan, R.A., 2002, A time frame for construction of the Kerguelen Plateau and Broken Ridge: Journal of Petrology, v. 43, p. 1109–1119, https://doi.org/10.1093/petrology/43.7.1109.

Du Vivier, A.D.C., Selby, D., Condon, D.J., Takashima, R., and Nishi, H., 2015, Pacific $^{187}Os/^{188}Os$ isotope chemistry and U-Pb geochronology: Synchroneity of global Os isotope change across OAE 2: Earth and Planetary Science Letters, v. 428, p. 204–216, https://doi.org/10.1016/j.epsl.2015.07.020.

Frey, F.A., Coffin, M., Wallace, P.J., and Weis, D., 2003, Leg 183 synthesis: Kerguelen Plateau-Broken Ridge—A large igneous province, *in* Frey, F.A., Coffin, M.F., Wallace, P.J., and Quilty, P.G., eds., Proceedings of the Ocean Drilling Program, Scientific Results, Volume 183: College Station, Texas, Ocean Drilling Program, p. 1–48, http://www-odp.tamu.edu/publications/183_SR/synth/synth.htm.

Gale, A.S., Kennedy, W.J., Burnett, J.A., Caron, M., and Kidd, B.E., 1996, The late Albian to early Cenomanian succession at Mont Risou near Rosans (Drôme, SE France): An integrated study (ammonites, inoceramids, planktonic foraminifera, nannofossils, oxygen and carbon isotopes): Cretaceous Research, v. 17, p. 515–606, https://doi.org/10.1006/cres.1996.0032.

Gale, A.S., Bown, P., Caron, M., Crampton, J., Crowhurst, S.J., Kennedy, W.J., Petrizzo, M.R., and Wray, D.S., 2011, The uppermost Middle and Upper Albian succession at the Col de Palluel, Hautes-Alpes, France: An integrated study (ammonites, inoceramid bivalves, planktonic foraminifera, nannofossils, geochemistry, stable oxygen and carbon isotopes, cyclostratigraphy): Cretaceous Research, v. 32, p. 59–130, https://doi.org/10.1016/j.cretres.2010.10.004.

Gale, A.S., Mutterlose, J., Batenburg, S., Gradstein, F.M., Agterberg, F.P., Ogg, J.G., and Petrizzo, M.R., 2020, The Cretaceous period, *in* Gradstein, F.M., Ogg, J.G., Schmitz, M.D., and Ogg, G.M., eds., Geologic Time Scale 2020: Amsterdam, Elsevier, p. 1023–1086, https://doi.org/10.1016/B978-0-12-824360-2.00027-9.

Gale, A.S., Kennedy, W.J., and Petrizzo, M.R., 2021, Stratigraphy of the Albian–Cenomanian boundary interval in the Agadir Basin, Morocco: Ammonites, microcrinoids, planktonic foraminifera: Acta Geologica Polonica, v. 71, no. 4, p. 453–480 m https://doi.org/10.24425/agp.2020.134560.

Gambacorta, G., Jenkyns, H.C., Russo, F., Tsikos, H., Wilson, P.A., Faucher, G., and Erba, E., 2015, Carbon- and oxygen-isotope records of mid-Cretaceous Tethyan pelagic sequences from the Umbria-Marche and Belluno Basins (Italy): Newsletters on Stratigraphy, v. 48, p. 299–323, https://doi.org/10.1127/nos/2015/0066.

Gambacorta, G., Malinverno, A., and Erba, E., 2019, Orbital forcing of carbonate versus siliceous productivity in the late Albian–early Turonian (Umbria-Marche Basin, central Italy): Newsletters on Stratigraphy, v. 52, p. 197–220, https://doi.org/10.1127/nos/2018/0456.

Gandolfi, R., 1942, Richerche micropaleontologiche e stratigrafiche sulla Scaglia e sul flysch Cretacici dei Dintorni di Balerna (Canton Ticino): Rivista Italiana di Paleontologia e Stratigrafia, v. 48, p. 1–160.

Grippo, A., Fischer, A.G., Hinnov, L.A., Herbert, T.D., and Silva, I.P., 2004, Cyclostratigraphy and chronology of the Albian stage (Piobbico core, Italy), *in* d'Argenio, B., Fischer, A.G., Premoli Silva, I., Weissert, H., and Ferreri, V., eds., Cyclostratigraphy: Approaches and Case Histories: Society for Sedimentary Geology (SEPM) Special Publication 81, p. 57–81, https://doi.org/10.2110/pec.04.81.0057.

Haq, B.U., 2014, Cretaceous eustasy revisited: Global and Planetary Change, v. 113, p. 44–58, https://doi.org/10.1016/j.gloplacha.2013.12.007.

Itoh, Y., Takano, O., and Takashima, R., 2017, Tectonic synthesis: A plate reconstruction model of the NW Pacific region since 100 Ma, *in* Itoh, Y., Dynamics of Arc Migration and Amalgamation—Architectural Examples from the NW Pacific Margin: Rijeka, Croatia, InTech, p. 93–111.

Jaffey, A., Flynn, K., Glendenin, L., Bentley, W.T., and Essling, A., 1971, Precision measurement of half-lives and specific activities of ^{235}U and ^{238}U: Physical Review C: Nuclear Physics, v. 4, p. 1889–1906, https://doi.org/10.1103/PhysRevC.4.1889.

Jarvis, I.A.N., Gale, A.S., Jenkyns, H.C., and Pearce, M.A., 2006, Secular variation in Late Cretaceous carbon isotopes: A new $\delta^{13}C$ carbonate reference curve for the Cenomanian–Campanian (99.6–70.6 Ma): Geological Magazine, v. 143, p. 561–608, https://doi.org/10.1017/S0016756806002421.

Jiang, Q., Jourdan, F., Olierook, H.K.H., Merle, R.E., and Whittaker, J.M., 2021, Longest continuously erupting large igneous province driven by plume-ridge interaction: Geology, v. 49, p. 206–210, https://doi.org/10.1130/G47850.1.

Jicha, B.R., Singer, B.S., and Sobol, P., 2016, Re-evaluation of the ages of $^{40}Ar/^{39}Ar$ sanidine standards and supereruptions in the western US using a Noblesse multi-collector mass spectrometer: Chemical Geology, v. 431, p. 54–66, https://doi.org/10.1016/j.chemgeo.2016.03.024.

Jones, M.M., Sageman, B.B., Selby, D., Jacobson, A.D., Batenburg, S.J., Riquier, L., MacLeod, K.G., Huber, B.T., Bogus, K.A., Tejada, M.L.G., and Kuroda, J., 2023, Abrupt episode of mid-Cretaceous ocean acidification triggered by massive volcanism: Nature Geoscience, v. 16, p. 169–174, https://doi.org/10.1038/s41561-022-01115-w.

Kawabe, F., 2000, Cretaceous stratigraphy in the Oyubari area, central Hokkaido, Japan: Bulletin of the National Museum of Nature and Science Series C: Geology & Paleontology, v. 26, p. 9–56.

Kawabe, F., Takashima, R., Wani, R., Nishi, H., and Moriya, K., 2003, Upper Albian to Lower Cenomanian biostratigraphy in the Oyubari area, Hokkaido, Japan: Toward a Cretaceous biochronology for the North Pacific: Acta Geologica Polonica, v. 53, p. 81–91.

Kennedy, W.J., 2020, Upper Albian, Cenomanian and Upper Turonian ammonite faunas from the Fahdène Formation of central Tunisia and correlatives in northern Algeria: Acta Geologica Polonica, v. 70, p. 147–272, https://doi.org/10.24425/agp.2019.126459.

Kennedy, W.J., Gale, A.S., Lees, J.A., and Caron, M., 2004, The global boundary stratotype section and point (GSSP) for the base of the Cenomanian Stage, Mont Risou, Hautes-Alpes, France: Episodes, v. 27, p. 21–32, https://doi.org/10.18814/epiiugs/2004/v27i1/003.

Kennedy, W.J., Cobban, W.A., Hancock, J.M., and Gale, A.S., 2005, Upper Albian and Lower Cenomanian ammonites from the Main Street Limestone, Grayson Marl and Del Rio Clay, Texas: Cretaceous Research, v. 26, p. 349–428, https://doi.org/10.1016/j.cretres.2004.11.018.

Krogh, T.E., 1973, A low-contamination method for hydrothermal decomposition of zircon and extraction of U and Pb for isotopic age determinations: Geochimica et Cosmochimica Acta, v. 37, p. 485–494, https://doi.org/10.1016/0016-7037(73)90213-5.

Kuiper, K.F., Deino, A., Hilgen, F.J., Krijgsman, W., Renne, P.R., and Wijbrans, A.J., 2008, Synchronizing rock clocks of Earth history: Science, v. 320, p. 500–504, https://doi.org/10.1126/science.1154339.

Leandro, C.G., Savian, J.F., Kochhann, M.V.L., Franco, D.R., Coccioni, R., Frontalini, F., Gardin, S., Jovane, L., Figueiredo, M., Tedeschi, L.R., and Janikian, L., 2022, Astronomical tuning of the Aptian stage and its implications for age recalibrations and paleoclimatic events: Nature Communications, v. 13, 2941, https://doi.org/10.1038/s41467-022-30075-3.

Lee, J.Y., Marti, K., Severinghaus, J.P., Kawamura, K., Yoo, H.S., Lee, J.B., and Kim, J.S., 2006, A redetermination of the isotopic abundances of atmospheric Ar: Geochimica et Cosmochimica Acta, v. 70, p. 4507–4512, https://doi.org/10.1016/j.gca.2006.06.1563.

Li, Y., Singer, B.S., Takashima, R., Schmitz, M.D., Podrecca, L.G., Sageman, B.B., Selby, D., Yamanaka, T., Mohr, M.T., Hayashi, K., and Tomaru, T., 2024, Radioisotopic chronology of ocean anoxic event 1a: Framework for analysis of driving mechanisms: Science Advances, v. 10, https://doi.org/10.1126/sciadv.adn8365.

Ma, C., Meyers, S.R., and Sageman, B.B., 2019, Testing Late Cretaceous astronomical solutions in a 15 million year astrochronologic record from North America: Earth and Planetary Science Letters, v. 513, p. 1–11, https://doi.org/10.1016/j.epsl.2019.01.053.

Malinverno, A., Erba, E., and Herbert, T.D., 2010, Orbital tuning as an inverse problem: Chronology of the early Aptian oceanic anoxic event 1a (Selli Level) in the Cismon APTICORE: Paleoceanography, v. 25, https://doi.org/10.1029/2009PA001769.

Matsumoto, H., Coccioni, R., Frontalini, F., Shirai, K., Jovane, L., Trindade, R., Savian, J.F., and Kuroda, J., 2022, Mid-Cretaceous marine Os isotope evidence for heterogeneous cause of oceanic anoxic events: Nature Communications, v. 13, 239, https://doi.org/10.1038/s41467-021-27817-0.

Matsumoto, T., Inoma, A., and Kawashita, Y., 1999, The turrilitid ammonoid *Mariella* from Hokkaido—Part 1 (Studies of the Cretaceous ammonites from Hokkaido and Sakhalin 85): Paleontological Research, v. 3, p. 106–120, https://doi.org/10.2517/prpsj.3.106.

Matsumoto, T., Takashima, R., AND Hasegawa, K., 2000, Some turrilitid ammonoids from the mid-Cretaceous of the Shuparo Valley, central Hokkaido (Studies of the Cretaceous ammonites from Hokkaido and Sakhalin 88): Bulletin of the Mikasa City Museum, Natural Science, no. 4, p. 1–13.

Matsumoto, T., Nishida, T., and Toshimitsu, S., 2003, Early Cenomanian (Cretaceous) ammonoids *Utaturiceras* and *Graysonites* from Hokkaido, north Japan (Studies of the Cretaceous ammonites from Hokkaido and Sakhalin-XCV): Bulletin of the Geological Survey of Japan, v. 54, p. 131–159, https://doi.org/10.9795/bullgsj.54.131.

Matsumoto, T., Nishida, T., and Toshimitsu, S., 2004, The early Cenomanian (Cretaceous) ammonite fauna from the Soeushinai area of Hokkaido, north Japan (Studies of the Cretaceous ammonites from Hokkaido and Sakhalin-XCVII): Bulletin of the Geological Survey of Japan, v. 55, p. 67–92, https://doi.org/10.9795/bullgsj.55.67.

Mattinson, J.M., 2005, Zircon U-Pb chemical abrasion ("CA-TIMS") method: Combined annealing and multi-step partial dissolution analysis for improved precision and accuracy of zircon ages: Chemical Geology, v. 220, p. 47–66, https://doi.org/10.1016/j.chemgeo.2005.03.011.

McLean, N.M., Condon, D.J., Schoene, B., and Bowring, S.A., 2015, Evaluating uncertainties in the calibration of isotopic reference materials and multi-element isotopic tracers (EARTHTIME tracer calibration part II): Geochimica et Cosmochimica Acta, v. 164, p. 481–501, https://doi.org/10.1016/j.gca.2015.02.040.

Mercer, C.M., and Hodges, K.V., 2016, ArAR—A software tool to promote the robust comparison of K-Ar and $^{40}Ar/^{39}Ar$ dates published using different decay, isotopic, and monitor-age parameters: Chemical Geology, v. 440, p. 148–163, https://doi.org/10.1016/j.chemgeo.2016.06.020.

Meyers, S.R., Siewert, S.E., Singer, B.S., Sageman, B.B., Condon, D.J., Obradovich, J.D., Condon, D.J., Jicha, B.R., and Sawyer, D.A., 2012, Intercalibration of radioisotopic and astrochronologic time scales for the Cenomanian-Turonian boundary interval, Western Interior Basin, USA: Geology, v. 40, p. 7–10, https://doi.org/10.1130/G32261.1.

Min, K., Mundil, R., Renne, P.R., and Ludwig, K.R., 2000, A test for systematic errors in $^{40}Ar/^{39}Ar$ geochronology through comparison with U/Pb analysis of a 1.1-Ga rhyolite: Geochimica et Cosmochimica Acta, v. 64, p. 73–98, https://doi.org/10.1016/S0016-7037(99)00204-5.

Obradovich, J.D., 1993, A Cretaceous time scale, *in* Caldwell, W.G.E., and Kauffman, E.G., eds., Evolution of the Western Interior Basin: Geological Association of Canada Special Paper 39, p. 379–396.

Obradovich, J.D., Matsumoto, T., Nishida, T., and Inoue, Y., 2002, Integrated biostratigraphic and radiometric study on the Lower Cenomanian (Cretaceous) of Hokkaido, Japan: Proceedings of the Japan Academy Series B: Physical and Biological Sciences, v. 78, p. 149–153, https://doi.org/10.2183/pjab.78.149.

Petrizzo, M.R., and Gilardoni, S.E., 2020, Planktonic foraminiferal biostratigraphy of late Albian–Cenomanian pelagic sequences from the Umbria-Marche Basin (central Italy) and the Mazagan Plateau (northeast Atlantic Ocean): Rivista Italiana di Paleontologia e Stratigrafia, v. 126, no. 3, p. 865–904.

Petrizzo, M.R., Caron, M., and Silva, I.P., 2015, Remarks on the identification of the Albian/Cenomanian boundary and taxonomic clarification of the planktonic foraminifera index species *globotruncanoides*, *brotzeni* and *tehamaensis*: Geological Magazine, v. 152, p. 521–536, https://doi.org/10.1017/S0016756814000478.

Quidelleur, X., Paquette, J.L., Fiet, N., Takashima, R., Tiepolo, M., Desmares, D., Nishi, H., and Grosheny, D., 2011, New U-Pb (ID-TIMS and LA-ICPMS) and $^{40}Ar/^{39}Ar$ geochronological constraints of the Cretaceous geologic time scale calibration from Hokkaido (Japan): Chemical Geology, v. 286, p. 72–83, https://doi.org/10.1016/j.chemgeo.2011.03.009.

Sageman, B.B., Singer, B.S., Meyers, S.R., Siewert, S.E., Walaszczyk, I., Condon, D.J., Jicha, B.R., Obradovich, J.D., and Sawyer, D.A., 2014, Integrating $^{40}Ar/^{39}Ar$, U-Pb, and astronomical clocks in the Cretaceous Niobrara Formation, Western Interior Basin, USA: Geological Society of America Bulletin, v. 126, p. 956–973, https://doi.org/10.1130/B30929.1.

Schaen, A.J., et al., 2021, Interpreting and reporting $^{40}Ar/^{39}Ar$ geochronologic data: Geological Society of America Bulletin, v. 133, p. 461–487, https://doi.org/10.1130/B35560.1.

Schmitz, M.D., and Schoene, B., 2007, Derivation of isotope ratios, errors and error correlations for U-Pb geochronology using ^{205}Pb-^{235}U-(^{233}U)-spiked isotope dilution thermal ionization mass spectrometric data: Geochemistry, Geophysics, Geosystems, v. 8, https://doi.org/10.1029/2006GC001492.

Scott, R.W., Oboh-Ikuenobe, F.E., Benson, D.G., Jr., Holbrook, J.M., and Alnahwi, A., 2018, Cenomanian-Turonian flooding cycles: US Gulf Coast and western interior: Cretaceous Research, v. 89, p. 191–210, https://doi.org/10.1016/j.cretres.2018.03.027.

Selby, D., and Creaser, R.A., 2003, Re-Os geochronology of organic rich sediments: An evaluation of organic matter analysis methods: Chemical Geology, v. 200, p. 225–240, https://doi.org/10.1016/S0009-2541(03)00199-2.

Selby, D., Mutterlose, J., and Condon, D.J., 2009, U-Pb and Re-Os geochronology of the Aptian/Albian and Cenomanian/Turonian stage boundaries: Implications for timescale calibration, osmium isotope seawater composition and Re-Os systematics in organic-rich sediments: Chemical Geology, v. 265, p. 394–409, https://doi.org/10.1016/j.chemgeo.2009.05.005.

Sigal, J., 1948, Notes sur les genres de foraminifères *Rotalipora* Brotzen 1942 et *Thalmanninella*, Famille des Globorotaliidae: Revue de l'Institut Français du Pétrole et Annales des Combustibles Liquides, v. 3, p. 95–103.

Singer, B.S., Jicha, B.R., Sawyer, D., Walaszczyk, I., Buchwaldt, R., and Mutterlose, J., 2021, Geochronology of late Albian–Cenomanian strata in the US Western Interior: Geological Society of America Bulletin, v. 133, p. 1665–1678, https://doi.org/10.1130/B35794.1.

Singer, B.S., Jicha, B.R., Sawyer, D.A., Walaszczyk, I., Landman, N., Sageman, B.B., and McKinney, K.C., 2025, A $^{40}Ar/^{39}Ar$ and U-Pb timescale for the Cretaceous Western Interior Basin, North America, *in* Hart, M.B., et al., eds., Cretaceous Project 200 Volume 1: The Cretaceous World: Geological Society, London, Special Publication 544, p. 367–391, https://doi.org/10.1144/SP544-2023-76.

Smoliar, M.I., Walker, R.J., and Morgan, J.W., 1996, Re-Os ages of group IIA, IIIA, IVA, and IVB iron meteorites: Science, v. 271, p. 1099–1102, https://doi.org/10.1126/science.271.5252.1099.

Takashima, R., Nishi, H., Yamanaka, T., Orihashi, Y., Tsujino, Y., Quidelleur, X., Hayashi, K., Sawada, K., Nakamura, H., and Ando, T., 2019, Establishment of Upper Cretaceous bio- and carbon isotope stratigraphy in the northwest Pacific Ocean and radiometric ages around the Albian/Cenomanian, Coniacian/Santonian and Santonian/Campanian boundaries: Newsletters on Stratigraphy, v. 52, p. 341–376, https://doi.org/10.1127/nos/2019/0472.

Takashima, R., Selby, D., Yamanaka, T., Kuwahara, Y., Nakamura, H., Sawada, K., Ikeda, M.A., Ando, T., Hayashi, K., Nishida, M., Usami, T., Kameyama, D., Nishi, H., Kuroyanagi, A., and Gyawali, B.R., 2024, Large igneous province activity drives oceanic anoxic event 2 environmental change across eastern Asia: Communications Earth & Environment, v. 5, p. 85, https://doi.org/10.1038/s43247-024-01214-z.

Tejada, M.L.G., Suzuki, K., Kuroda, J., Coccioni, R., Mahoney, J.J., Ohkouchi, N., Sakamoto, T., and Tatsumi, Y., 2009, Ontong Java Plateau eruption as a trigger for the early Aptian oceanic anoxic event: Geology, v. 37, p. 855–858, https://doi.org/10.1130/G25763A.1.

Thompson, W.R., 1935, On a criterion for the rejection of observations and the distribution of the ratio of deviation to sample standard deviation: Annals of Mathematical Statistics, v. 6, p. 214–219, https://doi.org/10.1214/aoms/1177732567.

Westerhold, T., Dallanave, E., Penman, D., Schoene, B., Röhl, U., Gussone, N., and Kuroda, J., 2025, Earth orbital rhythms links timing of Deccan Trap volcanism phases and global climate change: Science Advances, v. 11, no. 10, https://doi.org/10.1126/sciadv.adr8584.

Wilson, P.A., and Norris, R.D., 2001, Warm tropical ocean surface and global anoxia during the mid-Cretaceous period: Nature, v. 412, p. 425–429, https://doi.org/10.1038/35086553.

Yao, H., Chen, X., Melinte-Dobrinescu, M.C., Wu, H., Liang, H., and Weissert, H., 2018, Biostratigraphy, carbon isotopes and cyclostratigraphy of the Albian-Cenomanian transition and oceanic anoxic event 1d in southern Tibet: Palaeogeography, Palaeoclimatology, Palaeoecology, v. 499, p. 45–55, https://doi.org/10.1016/j.palaeo.2018.03.005.

Yao, H., Chen, X., Yin, R., Grasby, S.E., Weissert, H., Gu, X., and Wang, C., 2021, Mercury evidence of intense volcanism preceded oceanic anoxic event 1d: Geophysical Research Letters, v. 48, https://doi.org/10.1029/2020GL091508.

Science Editor: Troy Rasbury
Associate Editor: Catherine Mottram

Manuscript Received 28 April 2025
Revised Manuscript Received 16 September 2025
Manuscript Accepted 17 October 2025